Reduced Fresnel losses in chalcogenide fibers by using anti-reflective surface structures on fiber end faces

Jasbinder Sanghera,[1*] Catalin Florea,[2] Lynda Busse,[1] Brandon Shaw,[1] Fritz Miklos[2], and Ishwar Aggarwal,[1]

[1]US Naval Research Lab, Washington, DC 20375, USA
[2]GTEC Inc, Crofton, Maryland 21114, USA
**sanghera@nrl.navy.mil*

Abstract: We demonstrate microstructuring of chalcogenide fiber end faces in order to obtain enhanced transmission due to the antireflective properties of the microstructured surfaces. A variety of molding approaches have been investigated for As_2S_3 and As_2Se_3 fibers. Transmission as high as 97% per facet was obtained in the case of As_2S_3 fiber, compared to the native, Fresnel-loss limited, transmission of 83%. The potential for hydrophobic character was also demonstrated by increasing the contact angle of water droplets to greater than 120°.

OCIS codes: (060.2390) Fiber optics, infrared; (050.2065) Effective medium theory; (120.4610) Optical fabrication.

References and links

1. M. Born, and E. Wolf, *Principles of Optics*, 7th ed. (Cambridge University Press, 1999) Chapt. 1, pp. 54–74.
2. P. van der Werf, and J. Haisma, "Broadband antireflective coatings for fiber-communication optics," Appl. Opt. **23**(3), 499–503 (1984).
3. L. Rayleigh, "On the reflection of vibrations at the confines of two media between which the transition is gradual," Proc. Lond. Math. Soc. **11**(1), 51–56 (1879).
4. W. H. Southwell, "Pyramid-array surface-relief structures producing antireflection index matching on optical surfaces," J. Opt. Soc. Am. A **8**(3), 549–553 (1991).
5. A. B. Harker, and J. F. DeNatale, ""Diamond gradient index "moth-eye" antireflection surfaces for LWIR windows," Proc. SPIE **1760**, 261–267 (1992).
6. M. E. Motamedi, W. H. Southwell, and W. J. Gunning, "Antireflection surfaces in silicon using binary optics technology," Appl. Opt. **31**(22), 4371–4376 (1992).
7. C. G. Bernhard, and W. H. Miller, "A corneal nipple pattern in insect compound eyes," Acta Physiol. Scand. **56**(3-4), 385–386 (1962).
8. D. Hobbs, and B. D. MacLeod, "Design, Fabrication, and Measured Performance of Anti-Reflecting Surface Textures in Infrared Transmitting Materials," Proc. SPIE **5786**, 349–364 (2005).
9. P. Lalanne, and G. M. Morris, "Antireflection behavior of silicon subwavelength periodic structures for visible light," Nanotechnology **8**(2), 53–56 (1997).
10. M. Bitzer, J. Zosel, and M. Gebhardt, "Replication and surface enhancement of microstructured optical components," Proc. SPIE **5965**, 5965021–5965027 (2005).
11. Y. M. Song, S. Y. Bae, J. S. Yu, and Y. T. Lee, "Closely packed and aspect-ratio-controlled antireflection subwavelength gratings on GaAs using a lenslike shape transfer," Opt. Lett. **34**(11), 1702–1704 (2009).
12. Damage threshold at 10.6 microns in AMTIR2 glass for example was almost two times larger when patterned with motheye structure compared to when the substrate is left bare. [TelAztec, personal communication (2010)].
13. C. Viets, and W. Hill, "Comparison of fibre-optic SERS sensors with differently prepared tips," Sens. Actuators B Chem. **51**(1-3), 92–99 (1998).
14. G. Kostovski, D. J. White, A. Mitchell, M. W. Austin, and P. R. Stoddart, "Nanoimprinting on Optical Fiber End Faces for Chemical Sensing", Proc. SPIE **7004**, 70042H1–70042H4 (2008).
15. J. Viheriälä, T. Niemi, J. Kontio, T. Rytkonen, and M. Pessa, "Fabrication of surface reliefs on facets of singlemode optical fibres using nanoimprint lithography," Electron. Lett. **43**(3), 150–151 (2007).
16. W. Barthlott, "Epidermal and seed surface characters of plants: systematic applicability and some evolutionary aspects," Nord. J. Bot. **1**(3), 345–355 (1981).

#134471 - $15.00 USD Received 1 Sep 2010; revised 4 Oct 2010; accepted 4 Oct 2010; published 6 Dec 2010

Report Documentation Page

Form Approved
OMB No. 0704-0188

1. REPORT DATE	2. REPORT TYPE	3. DATES COVERED
OCT 2010		**00-00-2010 to 00-00-2010**

4. TITLE AND SUBTITLE	5a. CONTRACT NUMBER
Reduced Fresnel losses in chalcogenide fibers by using anti-reflective surface structures on fiber end faces	5b. GRANT NUMBER
	5c. PROGRAM ELEMENT NUMBER
6. AUTHOR(S)	5d. PROJECT NUMBER
	5e. TASK NUMBER
	5f. WORK UNIT NUMBER
7. PERFORMING ORGANIZATION NAME(S) AND ADDRESS(ES) **Naval Research Laboratory,Washington,DC,20375**	8. PERFORMING ORGANIZATION REPORT NUMBER
9. SPONSORING/MONITORING AGENCY NAME(S) AND ADDRESS(ES)	10. SPONSOR/MONITOR'S ACRONYM(S)
	11. SPONSOR/MONITOR'S REPORT NUMBER(S)

12. DISTRIBUTION/AVAILABILITY STATEMENT
Approved for public release; distribution unlimited

13. SUPPLEMENTARY NOTES

14. ABSTRACT

We demonstrate microstructuring of chalcogenide fiber end faces in order to obtain enhanced transmission due to the antireflective properties of the microstructured surfaces. A variety of molding approaches have been investigated for As2S3 and As2Se3 fibers. Transmission as high as 97% per facet was obtained in the case of As2S3 fiber, compared to the native, Fresnel-loss limited, transmission of 83%. The potential for hydrophobic character was also demonstrated by increasing the contact angle of water droplets to greater than 120?.

15. SUBJECT TERMS

16. SECURITY CLASSIFICATION OF:			17. LIMITATION OF ABSTRACT	18. NUMBER OF PAGES	19a. NAME OF RESPONSIBLE PERSON
a. REPORT	b. ABSTRACT	c. THIS PAGE			
unclassified	**unclassified**	**unclassified**	**Same as Report (SAR)**	**9**	

17. D. L. Brundrett, E. N. Glytsis, and T. K. Gaylord, "Homogeneous layer models for high-spatial-frequency dielectric surface-relief gratings: conical diffraction and antireflection designs," Appl. Opt. **33**(13), 2695–2706 (1994).
18. D. H. Raguin, and G. M. Morris, "Antireflection structured surfaces for the infrared spectral region," Appl. Opt. **32**(7), 1154–1167 (1993).

1. Introduction

Optical fibers are of great interest for a variety of applications in the mid-infrared wavelength region (2-5 μm). Examples include sensing, imaging, medical treatment and material processing. For the mid-infrared regions and beyond, the choice of materials which can be used to draw optical fibers is limited to high-index materials, such as chalcogenide glasses. These materials have high refractive indices (2.4 – 2.8) and hence the light experiences high reflection losses, known as Fresnel losses, when it enters and exits the fiber (around 17% loss per interface at 2 μm for an index of 2.4).

The loss due to the abrupt change in refractive index is reduced by applying an antireflective coating on the fiber end face. Typically, these coatings take advantage of the interference phenomenon which occur in thin films [1] and therefore they can be designed to enhance the light transmission within a defined wavelength band (wherein constructive interference takes place), reducing the reflection on the fiber end [2]. While these coatings are fairly robust in the case of silica-based glasses, they are more problematic when infrared materials are considered. In the case of chalcogenide glasses, which cannot be subjected to very high temperatures, the coatings have poor adhesion to the glass and are rather sensitive to humidity. Additionally, they damage easily under intense laser radiation. This is also the case when one considers bulk transmission windows and other optics, such as lenses or prisms, used for free-space manipulation of light.

A real breakthrough would be the elimination of AR coatings to reduce surface reflection losses. Lord Rayleigh addressed the issue of how to eliminate light reflection from a surface [3]. He solved the problem mathematically by assuming a continuously changing index from air to the bulk optic, essentially varying the porosity from 100% in air to 0% in the bulk. While this is easy to do mathematically, it is not possible to fabricate such controlled porosity gradients into the surface of bulk optics. Instead, it is possible to produce structures on the surface of an optic that are generally periodic and consist of a collection of identical objects such as graded pyramids, cones or similar artifacts [4–6]. These structures can be modeled using effective medium theory and finite element analysis to explain the reduced reflection. Basically, if we take a slice, layer-by-layer from air to the substrate, the effective index varies continuously from air to the solid substrate and so there is no discontinuous interface to reflect from. The height of the protrusions should be greater than $\lambda/2$ to reduce reflection loss, and the periodicity should be less than $\lambda/2n$ to avoid diffraction effects, where λ is the wavelength of operation and n is the index of the substrate. Consequently, the designs are material and wavelength specific.

If these structures are periodic they are often referred to as "motheye" surface structures, otherwise they are called "random" or "stochastic" surface structures. The term "motheye" is derived from the natural world; it was observed almost 50 years ago that the eye of nocturnal insects (e.g., a moth) reflected little or no light, regardless of the wavelength or the angle at which incident light struck the eye surface [7]. Artificially-produced structures can then significantly reduce the transmission loss from an optical interface, as demonstrated extensively in the last few years for many materials and through a variety of techniques [8–11]. Additionally, they are shown to have higher resistance to damage from high-intensity laser illumination [12] which is of great interest for high-power applications.

While most of the work has been directed to bulk optics, little has been done in terms of creating similar structures directly onto the fiber ends. Most of the work has been focused on obtaining surface-enhanced fiber sensors [13] and the approaches are based on nano-

#134471 - $15.00 USD Received 1 Sep 2010; revised 4 Oct 2010; accepted 4 Oct 2010; published 6 Dec 2010

imprinting [14,15]. Furthermore, all the work has been done on silica fibers and fiber transmission was not studied.

Interestingly enough, the leaves of a lotus blossom are covered with protrusions that are on a similar size scale to the moth eye structures [16]. What is remarkable about the lotus leaf is that it has water shedding properties, i.e. it self-cleans [16]. The micron scale protrusions on the leaf surface change the contact angle of water droplets creating a hydrophobic surface. Consequently, water droplets just roll off the surface, and in doing so, remove surface contaminants producing a clean surface. Similar water shedding effects have been observed in polymer surfaces with man-made protrusions. This has not yet been investigated in chalcogenide glasses but could provide an excellent opportunity to enable similar self cleaning mechanisms in IR optics.

In this paper we present what we believe to be the first demonstration of antireflective surface microstructuring of chalcogenide fibers using the direct stamping method. Modeling of the obtained structures is provided along with experimental data which demonstrates enhanced transmission over a broad, mid-infrared wavelength range. In addition, we measure the contact angle of water on IR glass substrates before and after stamping the moth eye structure and demonstrate the increase in hydrophobicity of the surface.

2. Experimental details

The direct stamping method we developed uses a template (also called a "shim") which has the negative of the desired microstructure pattern. A variety of materials can be used as a template. The shims we used were designed for the 2 – 5 μm range and made from nickel or silicon patterned through photolitography and etching. We have also tested arrays of microscopic glass tubes and a simple silicon wafer, acid-etched to reveal characteristic nanostructures, as well as black silicon. These materials were used to probe the limits of the direct stamping process. For accurate analysis of the imprinted patterns we used scanning electron microscopy (SEM) as well as focused ion-beam (FIB) milling. The latter technique is required in order to evaluate the depth of a given feature. An ion beam (typically gallium) is used to mill out portions of the material, revealing a cross-section in the pattern. Depending on the material, a platinum layer needs to be deposited on top of the microstructure in order to protect the individual features during this procedure.

For the stamping process, the template or shim was pressed directly against the preheated fiber end, which was held for certain duration and then removed (the fiber does not stick to the shim hence no precautions are needed). The stamping parameters depend on the fiber characteristics (e.g. glass transition temperature, T_g) and on the type of pattern to be reproduced. For example, in the case of As_2S_3 fibers, typical temperatures are in the 220 – 240 °C range and the stamping time is about 10 - 30 seconds. As_2Se_3 fibers require lower temperatures due to their lower T_g. All fibers were cleaved before stamping. Slight bulging of the fiber end was observed during the stamping process. This became more pronounced if excess force was applied. The stamping was performed in air or vacuum and our experimental setup also has the capability to add a process gas of choice (for example, we kept the stamping chamber dry by flushing it with nitrogen gas). A schematic of the stamping chamber is shown in Fig. 1.

#134471 - $15.00 USD Received 1 Sep 2010; revised 4 Oct 2010; accepted 4 Oct 2010; published 6 Dec 2010

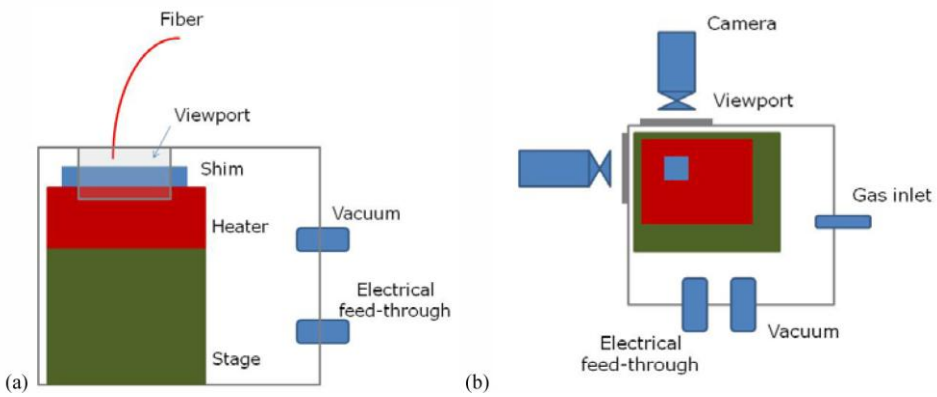

Fig. 1. Experimental setup used for direct stamping: (a) side view, (b) top view (attached fiber not shown in this view).

Fiber transmission, before and after the stamping, was measured using either a single-wavelength source (such as HeNe laser at 3.39 μm) or an FTIR spectrometer. The FTIR instrument (Analect Diamond-20) was custom modified to allow measurement of external samples (optical fibers in this case). Beam coupling at input and output is achieved using broadband, parabolic mirrors matching the NA of our fibers (in the range of 0.24 to 0.28). Most of our measurements were done on As_2S_3 fibers with 100 μm core and 170 μm clad diameters, but single-mode fibers with core diameters of 8 μm and other multimode fibers with core diameters of 50 μm were also stamped. The stamping was done one end at a time which allowed us to keep the other (input) end fixed. Therefore, coupling of light into the fiber did not change during the process and, hence, the measured transmission increase can be attributed solely to the microstructure created on the output fiber end. Slight changes in the fiber end face angle and the bulging observed as a result of the stamping process can introduce measurement errors, especially when using the FTIR. We were able to mitigate these issues by using an integrating sphere for the measurement at 3.39 μm and correcting the FTIR trace accordingly.

The contact angle of water droplets at room temperature and atmospheric pressure was measured before and after stamping of cleaved As_2S_3 fiber ends. In each case, the fiber end has been imaged with a telescope while a sprayer provided small droplets of de-ionized water. Video-frames were used to measure the contact angle using specialized software (Image-Pro Plus).

3. Stamping of various patterns

In order to evaluate the direct stamping process we used a variety of patterns with very small or deep or intricate features. For example, a rough side of a silicon wafer was acid-etched to reveal the characteristic pyramids and used as a stamp. Excellent reproduction was obtained, as illustrated in Fig. 2. Feature size of less than 200 nm can be easily observed. While this was not the focus of our work, it does demonstrate the feasibility for stamping nano-features into chalcogenide glass, and especially fibers.

#134471 - $15.00 USD Received 1 Sep 2010; revised 4 Oct 2010; accepted 4 Oct 2010; published 6 Dec 2010

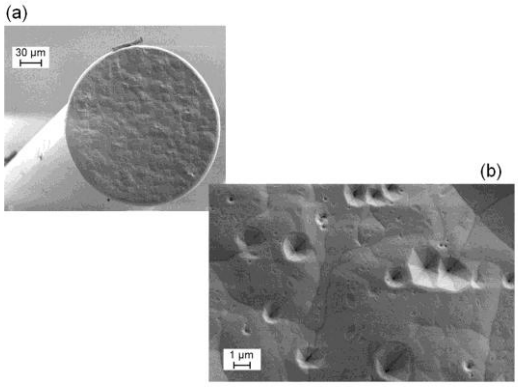

Fig. 2. SEM images of (a) stamped As_2S_3 fiber end, and (b) details of transferred structure on fiber end face. (30-µm and 1-µm markers, respectively).

A 2D array of large features was used to see how deep of a feature one can replicate. As illustrated in Fig. 3, depths of 10 – 20 µm are feasible. The direct stamping process has to be optimized in order to achieve the correct aspect ratio (period-to-depth ratio) of the features, this being very important when considering the antireflective properties of the replicated microstructure.

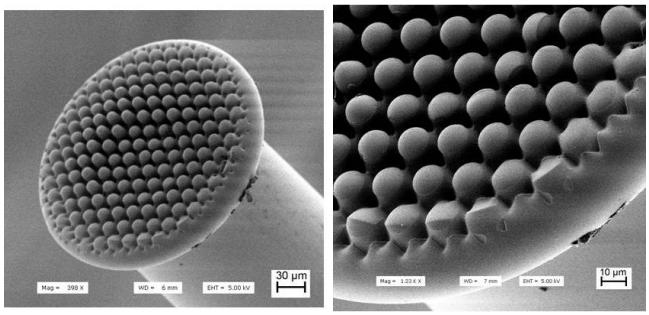

Fig. 3. SEM images of a stamped As_2S_3 fiber end - overview and detail. (30-µm and 10-µm markers, respectively).

4. Stamping of antireflective patterns

A variety of templates were used with the goal of reducing the Fresnel loss in the 2 – 5 µm region at the endface of multimode As_2S_3 fibers. The shims were designed using either TelAztec's proprietary software based on scattering theory [8], or they were designed in-house using a 2nd order approach to the effective medium theory [17]. The merits of the effective medium theory (EMT) have been discussed extensively in the literature and it has been shown that a 2nd order approach can yield fairly accurate results over a large range of parameters [17,18]. Three examples are detailed below showing representative types of shims which can be used for the above mentioned goal.

The most common type of motheye structure consists of a collection of small protuberances organized periodically in two dimensions. We will call such a shim a "positive" shim when the features are raised above the common surface. The nickel shim we used (designated as "28A") had hexagonally-packed protuberances with a pitch of 800 nm (the period, or feature separation, is around 920 nm.) and a feature height estimated around 900 to 1000 nm. As shown in Fig. 4 we were able to reproduce the pattern rather well.

#134471 - $15.00 USD Received 1 Sep 2010; revised 4 Oct 2010; accepted 4 Oct 2010; published 6 Dec 2010

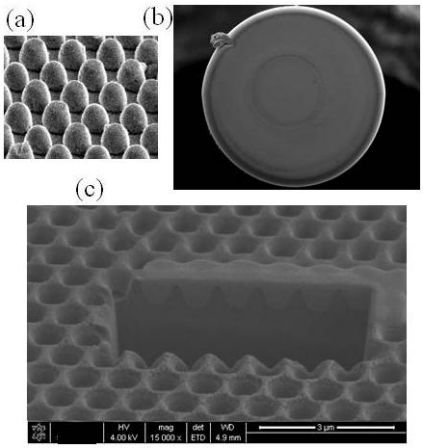

Fig. 4. As_2S_3 fiber end stamped using a positive nickel shim (28A): (a) profile of nickel shim, (b) overview of stamped fiber end, and (c) FIB image of the core area (3-μm marker); platinum was used as a milling protective layer.

Another type of shim we have tested consisted of a collection of depressions or holes. We call such a shim a "negative" shim since the features are below the common surface. The nickel shim (designated as "28B") had the holes also hexagonally-packed with a pitch of 800 nm and a feature depth estimated around 800 nm. Again, as shown in Fig. 5, we were able to reproduce the pattern rather well, especially when using moderate vacuum conditions (chamber pressure ~0.1 torr).

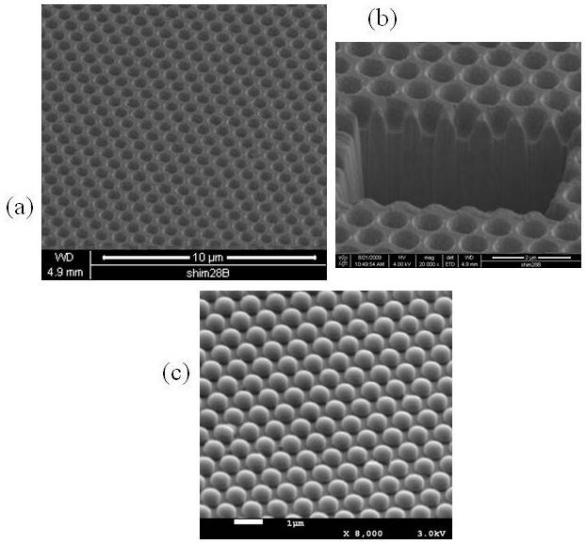

Fig. 5. As_2S_3 fiber end stamped using a negative nickel shim (28B): (a) profile of nickel shim, (b) FIB detail of the shim features (2-μm marker), (c) SEM image of the stamped fiber core area (1-μm marker).

Yet another type of shim we have tested consisted of a collection of spikes. The silicon shim (designated as "81104") had the spikes hexagonally-packed with a pitch of about 730 nm and a feature height estimated around 3000 nm. The replication was qualitatively good, as illustrated in Fig. 6. Even though we were not able to achieve the full aspect ratio of the original silicon pattern (depths obtained were in the 900 – 1300 nm range), the microstructured end did show reduction in the Fresnel loss. The poor performance obtained

#134471 - $15.00 USD Received 1 Sep 2010; revised 4 Oct 2010; accepted 4 Oct 2010; published 6 Dec 2010

with this shim might not be due to the poor aspect ratio but rather to the shape of the individual spikes.

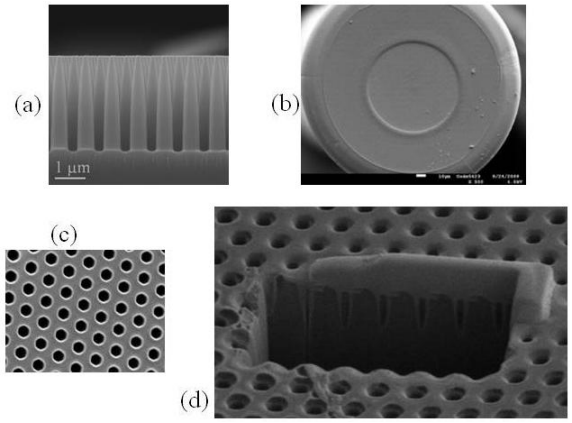

Fig. 6. As_2S_3 fiber end stamped using a positive silicon shim (81104): (a) profile of silicon pattern, (b) overview of stamped fiber end, (c) detail of pattern in the core area, (d) FIB image of the core area (platinum was used as a milling protective layer).

Typical values for one-end transmission as a consequence of the direct stamping process are given in Table 1 for all three cases. The data spread at 3.39 µm is obtained by measuring multiple samples. The original base transmission of the fiber end is estimated at 83% assuming the refractive index of the core is 2.4 for the As_2S_3 fiber used.

Table 1. Transmission values for fiber ends stamped with various shims (Transmission of unstamped fiber is approximately 83%).

Shim	Transmission at 3.39 µm	Maximum transmission
No Shim	~83%	~83%
28A	93.1% ± 1.9%	~94.5%
28B	94.3% ± 1.6%	~97.5%
81104	88.4% ± 1.4%	~89.8%

5. Investigation of hydrophobicity

We have also looked at how the surface hydrophobicity of the As_2S_3 glass changes when stamped with these types of patterns. Figure 7 shows the surface of a cleaved 170 µm diameter As_2S_3 glass fiber end after stamping a motheye structure using a positive nickel shim (negative image of shim 28B). As expected, the optical performance of this shim is comparable with shim 28B.

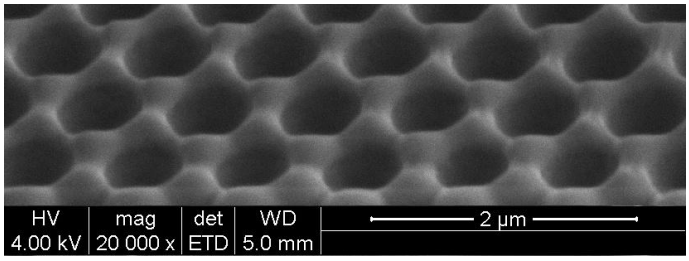

Fig. 7. Surface of a As_2S_3 glass fiber stamped with a positive nickel shim (SEM image at 52 degrees).

Furthermore, the contact angle on samples stamped with this pattern, as shown in Fig. 8, increases from 62° to over 120°, demonstrating the increase in the surface character from hydrophilic to superhydrophobic.

#134471 - $15.00 USD Received 1 Sep 2010; revised 4 Oct 2010; accepted 4 Oct 2010; published 6 Dec 2010

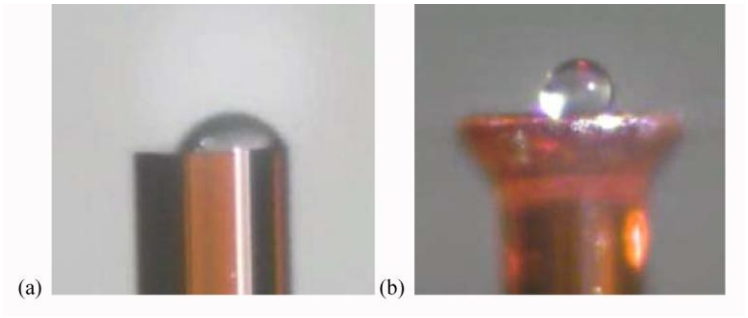

Fig. 8. Water droplet on surface of As_2S_3 glass fibers (a) cleaved surface (b) motheye-stamped surface.

6. Data analysis and conclusions

The best data was obtained with the nickel shim 28B and we have therefore concentrated our efforts toward data collection and theoretical modeling for fibers stamped with this shim. Careful data collection at 3.39 μm was correlated with the FTIR traces (by appropriate scaling) in order to obtain accurate transmission data for the 2 – 5 μm range. The experimental data was compared with modeling results obtained using the 2nd order EMT as shown in Fig. 9 below (index dispersion with the wavelength is taken into account).

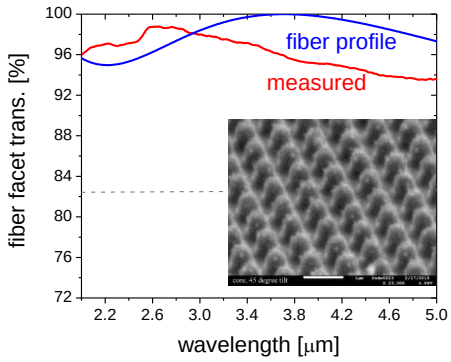

Fig. 9. Performance of stamped As_2S_3 fiber using shim 28B (feature height estimated at 849 nm). Inset shows patterned fiber end.

The experimentally measured data shows an abrupt decrease below 2.5 μm due to diffraction effects, as the wavelength of the probing light starts to be comparable with the feature period. It also shows a characteristic decrease at longer wavelengths, due to the fact that the depth of the stamped profile departs from optimum as the wavelength increases. While it is obvious that the EMT modeling is not a very accurate tool to precisely predict the performance of a given profile, it is nevertheless an easy tool for a quick estimation of such performance.

Further studies to compare various shims and processing conditions are under way. We are also refining the designs so as to obtain shims that will enable better transmission across the full 2 – 5 μm range, by shifting the diffraction edge toward smaller wavelengths and enhancing the aspect ratio of stamped profiles for consistent performance over the full spectral range of interest.

#134471 - $15.00 USD Received 1 Sep 2010; revised 4 Oct 2010; accepted 4 Oct 2010; published 6 Dec 2010

Acknowledgements

We thank TelAztec, Inc. for suggesting the design and providing the shim. Funding for this work was provided by the Joint Aircraft Survivability Program Office and the Test Resource Management Center through the Science and Technology/Test and Evaluation Program.

#134471 - $15.00 USD Received 1 Sep 2010; revised 4 Oct 2010; accepted 4 Oct 2010; published 6 Dec 2010